

Original Research Article

Enhanced removal of Cr(VI) by PEI/nFe₃O₄ ultrafiltration membranes using peristaltic pump-driven dynamic adsorption

ABSTRACT

In this study, Fe₃O₄ nanoparticles (nFe₃O₄) were loaded onto polyvinylidene fluoride ultrafiltration membranes and capped with polyethyleneimine in order to form PEI/nFe₃O₄ ultrafiltration membranes. We used a peristaltic pump as a driver for dynamic adsorption, and the PEI/nFe₃O₄ ultrafiltration membrane had a good ability to remove hexavalent chromium (Cr(VI)) from wastewater. The full permeate volume of the PEI/nFe₃O₄ ultrafiltration membrane was maximized at pH 3. Meanwhile, the removal of Cr(VI) from the wastewater reached 98% and reduced to trivalent chromium (Cr(III)). When the initial concentration of Cr(VI) increased, the active sites on the membrane would be filled and the removal efficiency of Cr(VI) would decrease. Meanwhile, the coexisting ions affect the removal efficiency of Cr(VI), and PO₄³⁻ has a strong negative effect on the removal efficiency. PEI/nFe₃O₄ ultrafiltration membrane is an effective combination of multifunctional nanomagnetic materials and membrane materials, which can effectively remove hexavalent chromium from wastewater. The study provides a basis for future applications in the environmental remediation of low-concentration chromium-containing wastewater.

Keywords: Nano Fe₃O₄ particles; Hexavalent chromium; Adsorption membrane; Heavy metal.

1. INTRODUCTION

Extensive use of heavy metals in industrial processes and the exploitation of natural resources has led to the gradual accumulation of these metals in surface water, causing a significant increase in water pollution over time[1]. The leather production, tanning, and electroplating industries extensively employ chromium[2]. Hexavalent chromium (Cr(VI)) is a highly toxic heavy metal ion and is recognized as a top priority for pollutant removal due to its toxicity, mutagenicity, and teratogenicity[3]. Cr(VI) is readily absorbed and accumulated in the human body, and even trace amounts of Cr(VI) can exert severe toxic effects on human health [4]. Therefore, it is very important to study the appropriate treatment method of Cr(VI). There

are various processing techniques for Cr (VI) (physical technology, chemical technology, etc.) [5-10]. Among various treatment technologies, ion exchange technology has a long history and requires high stability of exchange materials [11]; and electroflocculation technology has a high removal efficiency for Cr (VI) [12], and the selection of electrode materials is the key to this technology, and a large-scale power system is required [13]. Photocatalytic technology is widely used in the environmental field as an advanced technology [14-19], and can also achieve nearly 80% removal efficiency in Cr (VI) removal [20, 21]. Adsorption technology has gained significant attention in treating Cr(VI) wastewater due to its high purification efficiency, low energy consumption, economic benefits, and environmental friendliness [22].

The key to achieving high-efficiency adsorption lies in selecting adsorbents with a large specific surface area, high adsorption capacity, easy separation and regeneration, simple preparation, and high selectivity [23]. Nanocomposites have attracted attention in wastewater treatment due to their good selectivity, stability and large specific surface area [24]. Khalith et al. synthesized magnetite carbon nanocomposites using two agricultural wastes, achieving nearly 99% removal of Cr (VI) from wastewater at pH less than 5 [25]. A Fe_2O_3 -Ag nanocomposite was synthesized by Biswal et al. using the green method. This material has a monolayer adsorption capacity of 112.72 mg/g at pH 4 [26]. Multifunctional magnetic nanoparticles, with their large specific surface area, offer advantages over conventional adsorbents like graphene, activated carbon, and carbon nanotubes by providing more accessible and more efficient recovery after adsorption [27]. As an example, in one study it was found that water-soluble Fe_3O_4 nanoparticles were capable of adsorbing 90% of Pb^{2+} (10 ppm) within 2 minutes [28]. Various functionalized nano Fe_3O_4 ($n\text{Fe}_3\text{O}_4$) particles have been used to remove Cr(VI). Beheshti et al. prepared chitosan/MWCNT/ Fe_3O_4 composite nanofiber adsorbent by electrospinning method, and studied its removal efficiency of Cr (VI) ions in aqueous solution [29]. Wang et al. combined $n\text{Fe}_3\text{O}_4$ with reduced graphene oxide and polypyrrole to form a novel ternary magnetic composite with a maximum adsorption capacity of 293.3 mg/g for Cr(VI) [30]. Zabihi Sahebi et al. found that electrospun cellulose acetate/chitosan/single walled carbon nanotubes/ferrite/titanium dioxide nanofibers adsorbent have good removal ability for hexavalent chromium in systems containing Cr(VI), As(V), methylene blue and Congo red [31]. The versatile magnetic $n\text{Fe}_3\text{O}_4$ is a kind of typical multifunctional magnetic nanoparticles that uses its properties to minimize the latent risk of residual particles in the effluent [32].

Static adsorption exhibits long adsorption times and slow adsorption kinetics [22], while dynamic adsorption in membrane filtration shows promise in enhancing the efficiency of heavy metal wastewater treatment [33]. As a pressure-driven solute-solvent separation process, membrane filtration facilitates the entry of solutes into most adsorption sites, thereby enhancing the adsorption process [34].

Adsorption membranes are membrane materials utilized as adsorbents, including electrospun fiber membranes with large specific surface areas and high porosity, as well as

nano-reinforced membranes incorporating nanomaterials (such as the $n\text{Fe}_3\text{O}_4$ modified adsorption membrane and polymer-ceramic membranes composed of a combination of polymers and ceramics) [35, 36]. Previous studies have investigated the adsorption of Cr(VI) and divalent lead (Pb(II)) using nanofibrous membranes, and ultrafiltration experiments yielded the highest removal efficiency [37, 38]. Furthermore, an adsorption membrane operated by a peristaltic pump can efficiently remove heavy metals from wastewater within a short timeframe, offering a more cost-effective alternative to vacuum filtration and high-pressure ultrafiltration [34, 39].

In previous studies, versatile magnetic $n\text{Fe}_3\text{O}_4$ have rarely been combined with membrane materials. And dynamic adsorption is a feasible option. In this study, the surface functionalization of polyvinylidene fluoride (PVDF) membranes with $n\text{Fe}_3\text{O}_4$ and polyethyleneimine (PEI) was used to prepare a series of ultrafiltration membranes. The operation mode of dynamic adsorption, the effects of different initial Cr(VI) ion concentrations, coexisting ions and pH on Cr(VI) removal were investigated. The removal mechanism of Cr(VI) was analyzed to provide a basis for the effective treatment of Cr(VI)-containing wastewater.

2 METHODOLOGY

2.1 Materials

Ferric chloride hexahydrate (AR), ammonia (AR), anhydrous ethanol (AR), polyethyleneimine (99%), and ferric oxide nanoparticles were purchased from the Aladdin's Reagent Company (China). Ferrous sulfate heptahydrate, sulfuric acid and hydrochloric acid were obtained from the Sinopharm Reagent Company (China). PVDF membrane with a molecular weight of 100,000 Dalton (UF100) was supplied by the Zhongke Ruiyang Membrane Technology Co., Ltd. (Beijing, China).

2.2 Preparation of PEI/ $n\text{Fe}_3\text{O}_4$ modified ultrafiltration membranes

$n\text{Fe}_3\text{O}_4$ particles, prepared by co-precipitation, were placed in an ethanol solution and dispersed ultrasonically for 10 min. The mixture was then poured into an ultrafiltration cup with the commercial PVDF membrane positioned at the bottom (SI). The ethanol solution was allowed to flow out from a bottom filter port under a nitrogen pressure of 0.1 MPa, resulting in the deposition of $n\text{Fe}_3\text{O}_4$ particles on the surface of the PVDF membrane. Subsequently, the $n\text{Fe}_3\text{O}_4$ membranes were immersed in 1 wt% PEI solution for 5 min and subjected to thermal cross-linking and stabilization in an oven, resulting in the preparation of PEI/ $n\text{Fe}_3\text{O}_4$ ultrafiltration membranes. By controlling the mass of nanoparticles, we obtained modified membranes with nanoparticle loadings of 1 mg/cm^2 , 3 mg/cm^2 , 5 mg/cm^2 , 7 mg/cm^2 , and 9 mg/cm^2 . These membranes were designated as PEI/ $n\text{Fe}_3\text{O}_4$ -1, PEI/ $n\text{Fe}_3\text{O}_4$ -3, PEI/ $n\text{Fe}_3\text{O}_4$ -5, PEI/ $n\text{Fe}_3\text{O}_4$ -7 and PEI/ $n\text{Fe}_3\text{O}_4$ -9, respectively.

2.3 Continuous adsorption filtration experiments using Cr(VI) solution

Cr(VI) solution was pumped into an ultrafiltration cup (MSC300, Shanghai Mosu Science Equipment Co, Ltd). The effluent flow rate was maintained at a constant rotational speed throughout each experiment, and water samples were collected at specific filtration volumes or time intervals. Various parameters, including nFe₃O₄ loading, peristaltic pump speed, initial Cr(VI) concentration ranging from 5 mg/L to 200 mg/L, the presence of competing ions (Cl⁻, NO³⁻, SO₄²⁻, and PO₄³⁻), and pH value, which affected Cr(VI) removal, were investigated.

The permeate was then replaced with a 0.1 M NaOH solution, followed by three rinses using sufficient deionized water to clean the membranes and remove any residual eluent thoroughly. The reusability of the membranes was assessed by this process. Detailed procedures can be found in the Supplementary Information. The Cr(VI) removal efficiency (R) was calculated using the following equation:

$$R = \left(1 - \frac{C_p}{C_f}\right) \times 100\% \quad (1)$$

where C_p and C_f are the concentrations of heavy metal ions (mg/L) in the permeate and in the feed solution (initial concentration of 10 mg/L), respectively.

Two adsorption kinetic models, pseudo-first-order and pseudo-second-order, were used to analyze the Cr(VI) removal with PEI/nFe₃O₄-9 at different concentrations[40]:

$$q_t = q_e(1 - \exp(-k_1 t)) \quad (2)$$

$$q_t = \frac{k_2 q_e^2 t}{1 + k_2 q_e t} \quad (3)$$

where q_t and q_e are the adsorption amounts at time t and at the equilibrium time, respectively, and k_1 and k_2 are the pseudo-first-order model rate constants, pseudo-second-order rate constants, and intraparticle diffusion rate constants, respectively. Results are presented in Table 1.

Table 1. Two kinetic parameters of Cr(VI) ion adsorption using PEI/nFe₃O₄-9.

Cr(VI) concentrations (mg/L)	Pseudo-first-order			Pseudo-second-order		
	q _e (mg/mg)	k ₁ (1/min)	R ²	q _e (mg/mg)	k ₂ [mg/(mg·min)]	R ²
5	16.94	0.0136	0.9999	33.42	0.2301	0.9809
10	15.78	0.0293	0.9999	28.96	0.4641	0.9952
50	21.59	0.0898	0.9995	32.37	2.0885	0.9826

80	20.43	0.1510	0.9989	30.05	3.3627	0.9958
100	22.44	0.1712	0.9993	32.32	4.2396	0.9981
200	27.96	0.2250	0.9906	36.64	7.8003	0.9924

2.4 Sample analysis

The morphological characteristics of $n\text{Fe}_3\text{O}_4$ were analyzed using high-analysis transmission electron microscopy (TEM) (H-7650, Hitachi, Japan), and the particle size distribution was counted using ImageJ software. The crystal structure of the magnetic $n\text{Fe}_3\text{O}_4$ particles was determined using an X-ray diffractometer (XRD) (D8 Advance, Bruker, Germany) with $\text{K}\alpha$ -radiation of Cu targets in the range of 10 - 80° 2θ . The particles were tested using a thermal stability analyzer (TGA/SDTA 851E, METTLER TOLEDO, USA). The scanning range was 25 - 800°C , with a ramp rate of $10^\circ\text{C}/\text{min}$, under a nitrogen atmosphere. The structure of the PEI/ $n\text{Fe}_3\text{O}_4$ modified films and the distribution of $n\text{Fe}_3\text{O}_4$ were observed using a field emission environmental scanning electron microscope (SEM) (Quant 250, FEI, USA). Energy dispersive spectrometer (EDS) was used to qualitative or semi-quantitative compositional elemental analysis. X-ray photoelectron spectroscopy (XPS) (Thermo Scientific K-Alpha, Thermo Fisher Scientific, USA) was performed to determine the elemental valence of the membrane surface.

3 RESULTS AND DISCUSSION

3.1 Characterization of the $n\text{Fe}_3\text{O}_4$ -modified PVDF membrane

TEM images of the $n\text{Fe}_3\text{O}_4$ are presented in Figure 1A. The synthesized nanoparticles exhibited a uniform spherical structure, with a minor accumulation of $n\text{Fe}_3\text{O}_4$ particles. The particles formed large chain-like aggregates through interparticle interactions. The particle size distribution of the $n\text{Fe}_3\text{O}_4$ (Fig. 1B) ranged from 5 to 23 nm, with the majority falling within the 9 - 13 nm range. The $n\text{Fe}_3\text{O}_4$ particles were synthesized using the co-precipitation method. Their XRD pattern (Fig. 1B) exhibited peaks at 29.65° , 35.20° , 43.06° , 56.68° , and 62.38° , corresponding to the crystal planes (220), (311), (400), (511), and (440) of Fe_3O_4 [41]. These findings demonstrate that $n\text{Fe}_3\text{O}_4$ with a trans-spinel structure was successfully synthesized.

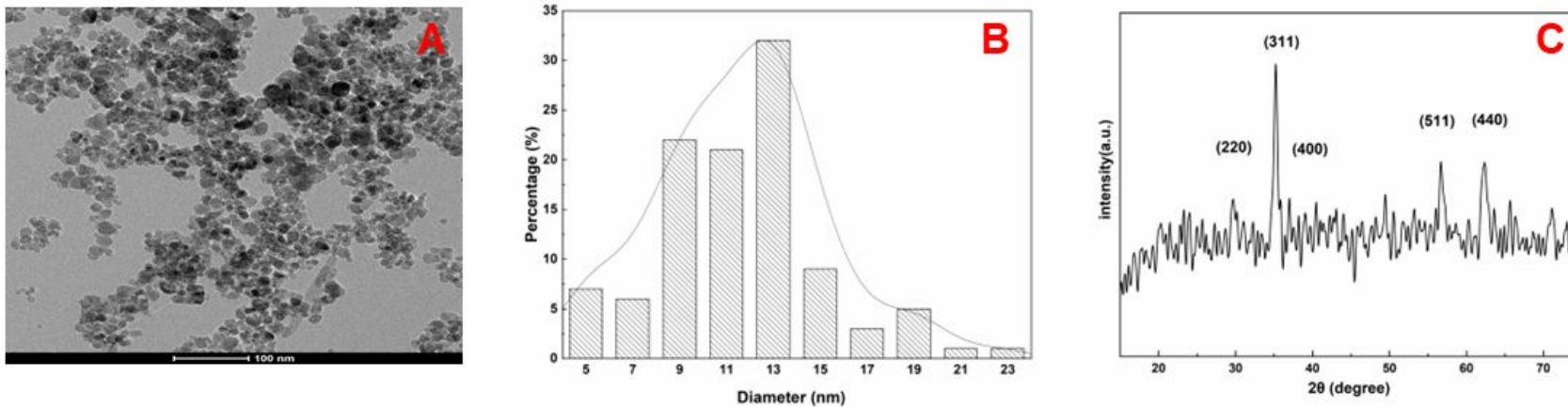


Figure 1. A) TEM image of $n\text{Fe}_3\text{O}_4$ particles. B) Histogram of the size distribution of $n\text{Fe}_3\text{O}_4$ nanoparticles. C) XRD pattern of the $n\text{Fe}_3\text{O}_4$ nanoparticles.

Figure 2 displays the surface morphological characteristics of the PEI/nFe₃O₄ ultrafiltration membrane using SEM imagery. With an increase in the nFe₃O₄ loading, a pronounced accumulation of particles occurred due to the strong magnetic interaction between the nFe₃O₄ particles, resulting in their accumulation and agglomeration on the membrane surface. At an nFe₃O₄ particle loading of 9 mg/cm² on the membrane surface, an increased porous structure was observed on the top of the membrane, accompanied by a non-uniform distribution of nFe₃O₄ particles. The EDS results revealed the presence of both Fe and N elements in the modified membrane (Fig. S1), confirming the successful loading of both nFe₃O₄ particles and PEI polymer onto the PVDF membrane surface.

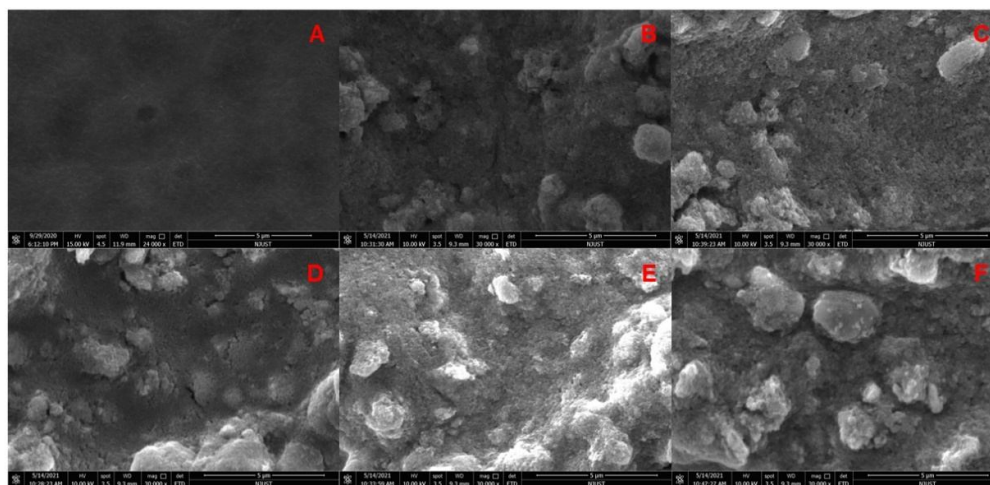


Figure 2. SEM imagery of PEI/nFe₃O₄ ultrafiltration membranes at different nFe₃O₄ nanoparticle loadings. A) Pure PVDF membrane. B) 1 mg/cm². C) 3 mg/cm². D) 5 mg/cm². E) 7 mg/cm². F) 9 mg/cm².

3.2 Cr(VI) removal

The efficiencies of PEI/nFe₃O₄ ultrafiltration membranes with varying loadings in treating chromium-containing wastewater under nitrogen pressure (0.1 MPa) and various peristaltic pump operational modes are presented in Fig. 3A. Under the peristaltic pump feed mode, the removal efficiencies of the modified membranes increased as the coating nanoparticle loading increased, reaching a maximum removal efficiency of 84.7%. In comparison, the removal efficiency under the nitrogen pressurization mode was only 52.0%. The observed differences in removal trends between the two operational modes might be attributed to variations in the residence times of the solution. The peristaltic pump mode exhibited superior removal of Cr(VI). Thus, subsequent experiments were conducted using this operational mode.

Removal efficiencies of Cr(VI) by the PEI/nFe₃O₄ ultrafiltration membranes at various peristaltic pump speeds are presented in Figures 3B and 3C. The filtration experiment at a peristaltic pump speed of 3 rpm achieved the highest Cr(VI) removal efficiency with a value of

87.5%. As the peristaltic pump speed increased to 5 rpm and then 7 rpm, the removal efficiency of Cr(VI) decreased to 85.8% and 84.7%, respectively. Thus, higher peristaltic pump speeds led to lower Cr(VI) removal efficiencies. However, slower rotational speeds led to lower filtrate permeation rates and significantly prolonged treatment times for contaminants. Thus, selecting an appropriate peristaltic pump speed is crucial to achieving a well-balanced purification performance of the PEI/nFe₃O₄ ultrafiltration membrane in treating heavy metal wastewater. Subsequent experiments were conducted at a peristaltic pump speed of 5 rpm.

UNDER PEER REVIEW

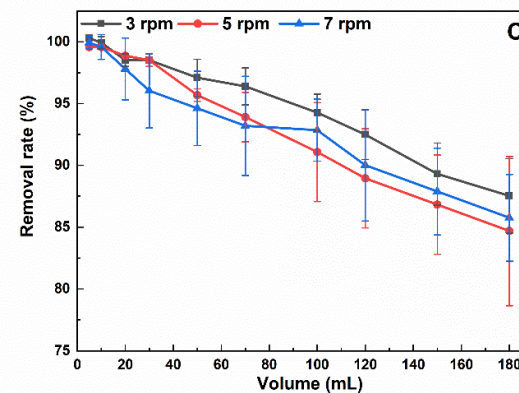
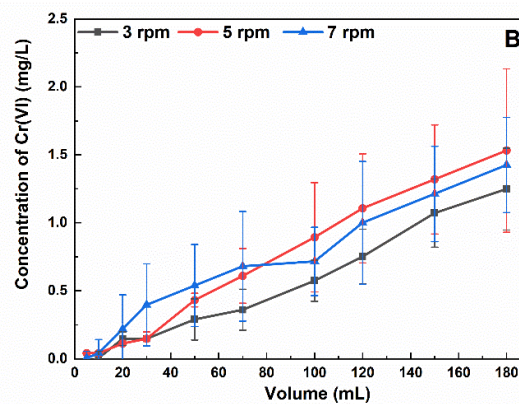
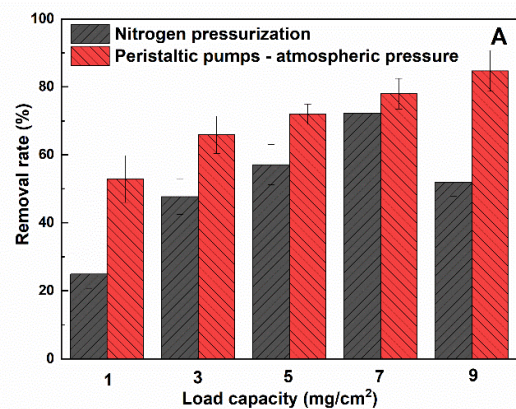


Figure 3. A) Effect of different operational modes and different $n\text{Fe}_3\text{O}_4$ nanoparticle loadings on Cr(VI) removal by PEI/ $n\text{Fe}_3\text{O}_4$ ultrafiltration membranes. B) Cr(VI) removal concentrations by PEI/ $n\text{Fe}_3\text{O}_4$ ultrafiltration membranes at different peristaltic pump rotational speeds. C) Cr(VI) removal efficiencies by PEI/ $n\text{Fe}_3\text{O}_4$ ultrafiltration membranes at different peristaltic pump rotational speeds.

3.3 Effect of nanoparticle loading and Cr(VI) concentration

The performance of the PEI/nFe₃O₄ ultrafiltration membranes with varying nanoparticle loadings for removing Cr(VI) is shown in Figures 4A and 4B. The PVDF membrane without nFe₃O₄ and PEI exhibited a low Cr(VI) removal efficiency with a value of 7.8%. The PEI/nFe₃O₄ membranes showed higher Cr(VI) removal efficiencies compared to that of the PVDF membrane, and the removal efficiencies gradually increased with nFe₃O₄ loading increased. The corresponding removal efficiencies with different nanoparticle loadings were 52.8%, 65.9%, 71.9%, 78.0%, and 84.7% for PEI/nFe₃O₄-1, PEI/nFe₃O₄-3, PEI/nFe₃O₄-5, PEI/nFe₃O₄-7 and PEI/nFe₃O₄-9, respectively.

The Cr(VI) removal efficiency by pure nFe₃O₄-9 particles was 69.7%. The PEI/nFe₃O₄-9 ultrafiltration membrane consistently maintained a high removal efficiency during dynamic adsorption and filtration, indicating the removal of Cr(VI) was enhanced through the one-step filtration adsorption process. The filtrate had a low total Fe concentration after multiple centrifugations following filtration, indicating that the N₂ pressurized preparation method and surface encapsulation of PEI effectively prevented the loss of surface nanoparticles.

Figure 3A demonstrates that the permeate volume reached its maximum at approximately 10% of the initial concentration and remained constant during the entire filtration process, which closely matched the total filtration volume of 180 mL. This result suggests that excellent Cr(VI) removal was achieved during filtration using the PEI/nFe₃O₄-9 ultrafiltration membrane. Consequently, further investigation focused on this membrane.

The Cr(VI) removal efficiencies of the PEI/nFe₃O₄-9 ultrafiltration membrane under various concentrations of Cr(VI) are presented in Figures 4C and 4D. The removal efficiencies exhibited varying degrees of reduction as Cr(VI) concentrations increased. The PEI/nFe₃O₄-9 membrane achieved removal efficiencies of 94.2%, 84.7%, 56.0%, 43.2%, 40.0%, and 27.6% when Cr(VI) concentrations ranged from 5 mg/L, 10 mg/L, 50 mg/L, 80 mg/L, 100 mg/L and 200 mg/L, respectively. The lowest removal efficiency, observed when the Cr(VI) concentration was 200 mg/L, might be attributed to the gradual saturation of the active sites of the membrane, which reached an upper limit of the modified membrane treatment and resulted in reduced removal of hexavalent chromium.

Figure 4C demonstrates a significant decrease in permeate volume as the initial concentration increased from 5 mg/L to 200 mg/L. An increase in the initial concentration of the solution resulted in a shorter time to reach the penetration point while causing only a slight change in the filtrate flow rate. During the middle and late stages of filtration, the increased amount of adsorbed Cr(VI) and the gradual accumulation of retained and adsorbed Cr(VI) in the pore channels of the inner layer of the membrane resulted in a broader mass transfer region (Fig. 4C). The one-step dynamic adsorption and filtration mode using the PEI/nFe₃O₄ membranes holds great promise for the efficient and rapid removal of Cr(VI) from low-concentration chromium-containing wastewater, making it a viable option for environmental remediation applications.

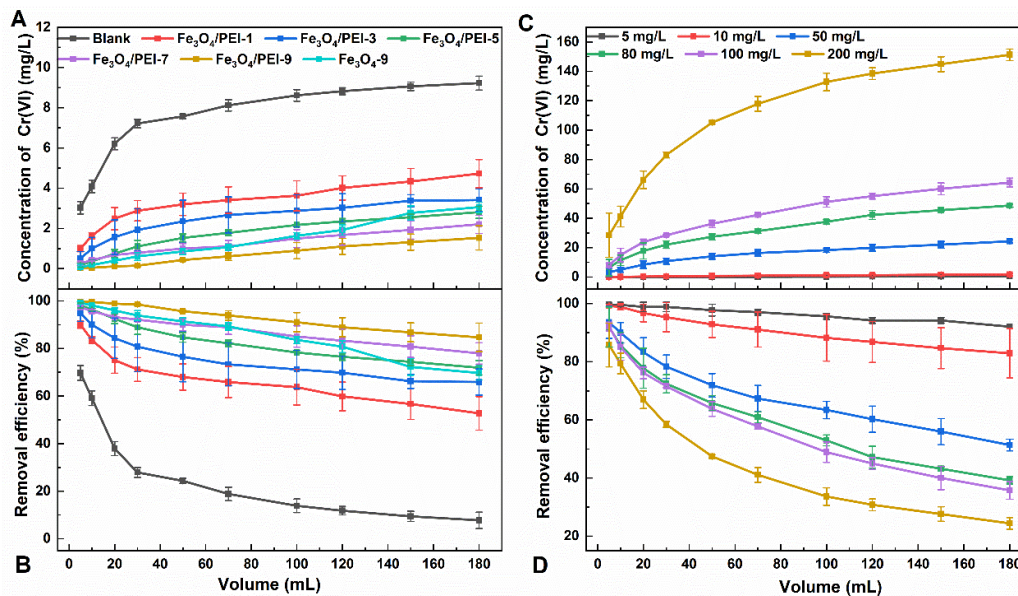


Figure 4. A) Concentrations of Cr(VI) removed by ultrafiltration membranes with different loadings of PEI/nFe₃O₄. B) Removal efficiencies of Cr(VI) by ultrafiltration membranes with different loadings of PEI/nFe₃O₄. C) Concentrations of Cr(VI) removed by the PEI/nFe₃O₄-9 ultrafiltration membrane under various concentrations of Cr(VI). D) Removal efficiencies of Cr(VI) removed by the PEI/nFe₃O₄-9 ultrafiltration membrane under various concentrations of Cr(VI).

The adsorption results were analyzed using pseudo-first-order and pseudo-second-order kinetic models, and the findings are presented in Table 1. The pseudo-second-order models exhibited an excellent fit to the Cr(VI) ion adsorption kinetic data, consistent with the pseudo-first-order kinetic model. Furthermore, PEI/nFe₃O₄-9 demonstrated the highest adsorption performance when treating a concentration of 200 mg/L of Cr(VI), corresponding to the adsorption capacity. The kinetic data indicated that Cr(VI) uptake using PEI/nFe₃O₄-9 was correlated with physical adsorption and chemical interaction [42].

It is worth noting that once chromium ions were adsorbed by the nanoparticles, some reduced Cr(III) might attach to the surface of the nFe₃O₄ particles, forming a passivation layer and occupying some active sites. The removal efficiency of hexavalent chromium showed an increasing trend with higher initial chromium ion concentrations. This can be attributed to the influence of the initial ion concentration of heavy metals on the driving force between the adsorbate (Cr(VI)) and the adsorbent material (PEI/nFe₃O₄). With the gradual increase in Cr(VI) concentration, the binding force between the ions and the adsorption sites on the membrane surface and within the pores became stronger. This enhanced the adsorption capacity of the PEI/nFe₃O₄-9 ultrafiltration membrane and improved the removal of Cr(VI).

3.4 Effect of coexisting ions and pH on Cr(VI) removal

The pH of the solution plays a crucial role in Cr(VI) removal by affecting the degree of protonation on the surface of the PEI/nFe₃O₄-9 ultrafiltration membrane and the physicochemical properties of the

Cr(VI). Figure 5A illustrates the significant impact of solution pH on removing Cr(VI). The PEI/nFe₃O₄-9 ultrafiltration membranes achieved a Cr(VI) removal efficiency of 91.1% at a pH of 1. The highest Cr(VI) removal efficiency of 99.2% was achieved at a pH of 3. As depicted in Figure 5B, with the initial concentration of 10% as the breakthrough point, PEI/nFe₃O₄-9 ultrafiltration membrane achieved the maximum value of the entire breakthrough volume at a pH of 3, showing a more excellent heavy metal ion removal ability. Nevertheless, increased pH resulted in a decline in Cr(VI) removal efficiency. The PEI/nFe₃O₄-9 ultrafiltration membrane displayed the lowest efficiency in Cr(VI) removal, reaching only 30.3% at pH 9.

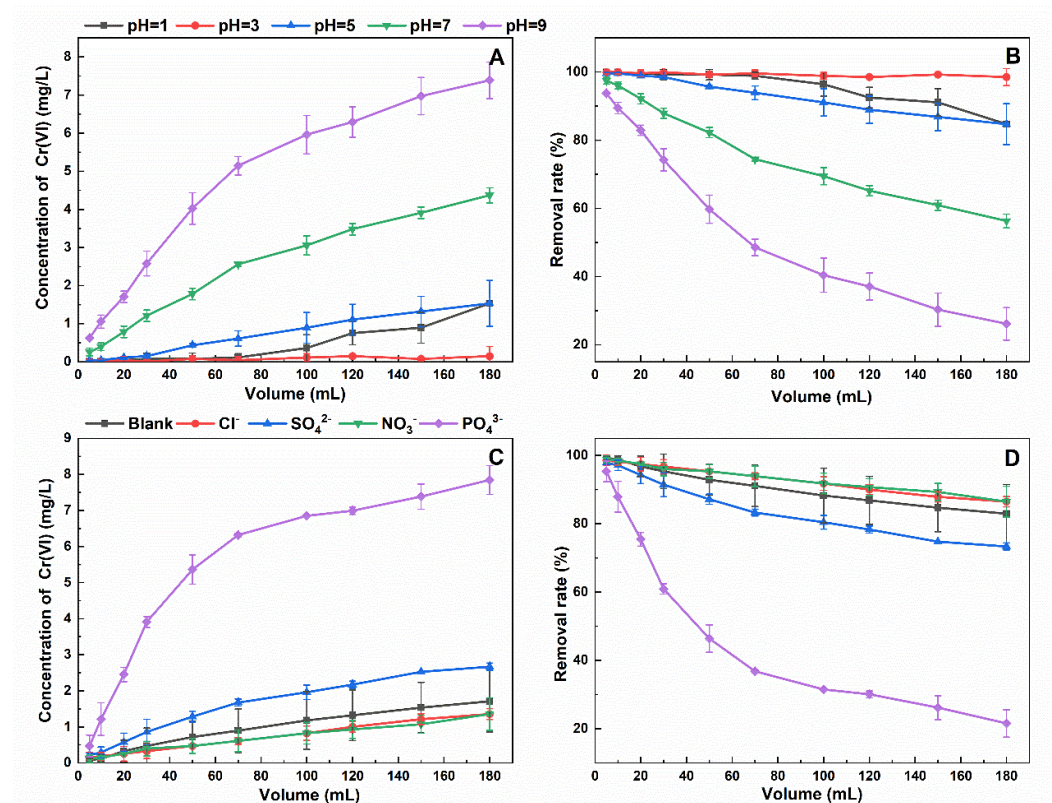


Figure 5. A) Concentrations of Cr(VI) removal by PEI/nFe₃O₄-9 ultrafiltration membranes at different values of pH. B) Removal efficiencies of Cr(VI) by PEI/nFe₃O₄-9 ultrafiltration membranes at different values of pH. C) Concentrations of Cr(VI) removal by PEI/nFe₃O₄-9 ultrafiltration membranes in the presence of interfering ions (Cl⁻, SO₄²⁻, NO₃⁻ and PO₄³⁻). D) Removal efficiencies of Cr(VI) by PEI/nFe₃O₄-9 ultrafiltration membranes in the presence of interfering ions (Cl⁻, SO₄²⁻, NO₃⁻ and PO₄³⁻). Cr(VI) existed in various forms in solution, including HCrO₄⁻, CrO₄²⁻, Cr₂O₇²⁻, and Cr(VI), with the ions HCrO₄⁻, CrO₄²⁻, and Cr₂O₇²⁻ being predominant at pH 2 to 6 [43]. The PEI molecular chain on the membrane surface contains rich amine groups, which readily undergo protonation and acquire a positive charge under acidic conditions. This facilitates stronger electrostatic attraction to the negatively charged anions HCrO₄⁻ and Cr₂O₇²⁻[44]. However, the removal efficiency of Cr(VI) by the modified membrane decreased at pH 1 compared with that at pH 3. This can be attributed to the transformation of Cr(VI) from HCrO₄⁻ to H₂CrO₄, where the altered molecular form is not conducive to adsorption by the positively charged polymeric material. When the pH was greater than 6, the predominant form of Cr(VI)

was the CrO_4^{2-} ion, necessitating an increased presence of positively charged groups for efficient adsorption of CrO_4^{2-} owing to its higher ionic valence [45]. Furthermore, as the concentration of OH^- increased, the protonation on the membrane decreased while the negative charge increased, thereby hindering the adsorption of Cr(VI) anions. Simultaneously, Cr(VI) was reduced to Cr(III) while adsorbing onto the $\text{PEI/nFe}_3\text{O}_4$.

The following equations demonstrate the reactions involved in the participation of H^+ as a reactant [46]:



According to equation (6), when HCrO_4^- predominated as the primary form of Cr(VI) in the solution, its conversion to Cr(III) primarily occurred through reduction. At pH 9, Cr(VI) predominantly existed as CrO_4^{2-} ions, following the conversion pathway described in equation (5). Simultaneously, the generated Cr(III) within the interlayer of the membrane underwent passivation on the particle surface, resulting in the formation of Cr(OH)_3 precipitates. This process diminishes the effectiveness of the modified membrane in Cr(VI) removal [47].

The presence of coexisting ions Cl^- , SO_4^{2-} , NO_3^- and PO_4^{3-} in the solution resulted in removal efficiencies for Cr(VI) of 73.0%, 71.9%, 64.5%, and 14.5%, respectively, when employing the $\text{PEI/nFe}_3\text{O}_4$ -9 ultrafiltration membranes (Fig. 5D). The order of coexisting anions in terms of their impact on the removal efficiency of Cr(VI) was $\text{PO}_4^{3-} > \text{SO}_4^{2-} > \text{Cl}^- > \text{NO}_3^-$. In comparison to the absence of competing ions, Cl^- and NO_3^- exhibited a marginal contribution to the removal efficiency of Cr(VI) , potentially attributed to their capability of promoting the reduction of Cr(VI) by nFe_3O_4 [48]. The presence of PO_4^{3-} ions notably diminished the removal capacity of Cr(VI) .

The impact of coexisting ions on the removal efficiency can be elucidated in several ways. The negatively charged Cr(VI) ions may have been adsorbed onto the surface of positively charged PEI polymer adsorption sites, resulting in inevitable competition between coexisting anions and Cr(VI) [49]. Furthermore, the competition between coexisting ions and Cr(VI) was influenced by their ionic valence and chemical structure [50, 51]. Cl^- and NO_3^- formed weak outer-sphere surface complexes, leading to minimal competition during Cr(VI) uptake [52]. Moreover, monovalent anions such as NO_3^- and Cl^- exhibited weaker ionic energies and electrostatic adsorption than divalent and trivalent anions. This study observed that SO_4^{2-} and PO_4^{3-} demonstrated higher competitiveness for positively charged surfaces, resulting in decreased Cr(VI) reduction at the reaction sites and diminished adsorption capacity of chromium ions. These findings suggest that highly charged anions effectively bind to reactive sites and display greater competitiveness towards Cr(VI) .

3.5 The Cr(VI) removal mechanism

XPS analysis was performed on the surface of the PEI/nFe₃O₄-9 ultrafiltration membrane to investigate its surface chemistry (Fig. 6). The presence of Fe, O, and N core energy levels indicated the main elemental composition of the membrane surface, confirming the presence of PEI on the PEI/nFe₃O₄ ultrafiltration membrane surface. A new peak attributed to Cr appeared around 570-595 eV, confirming the successful adsorption of Cr(VI). Furthermore, the N1s peak displayed a higher binding energy shift and a considerable decrease in intensity after adsorption, suggesting the participation of the amine group of the PEI chain in Cr(VI) removal and its strong binding capability.

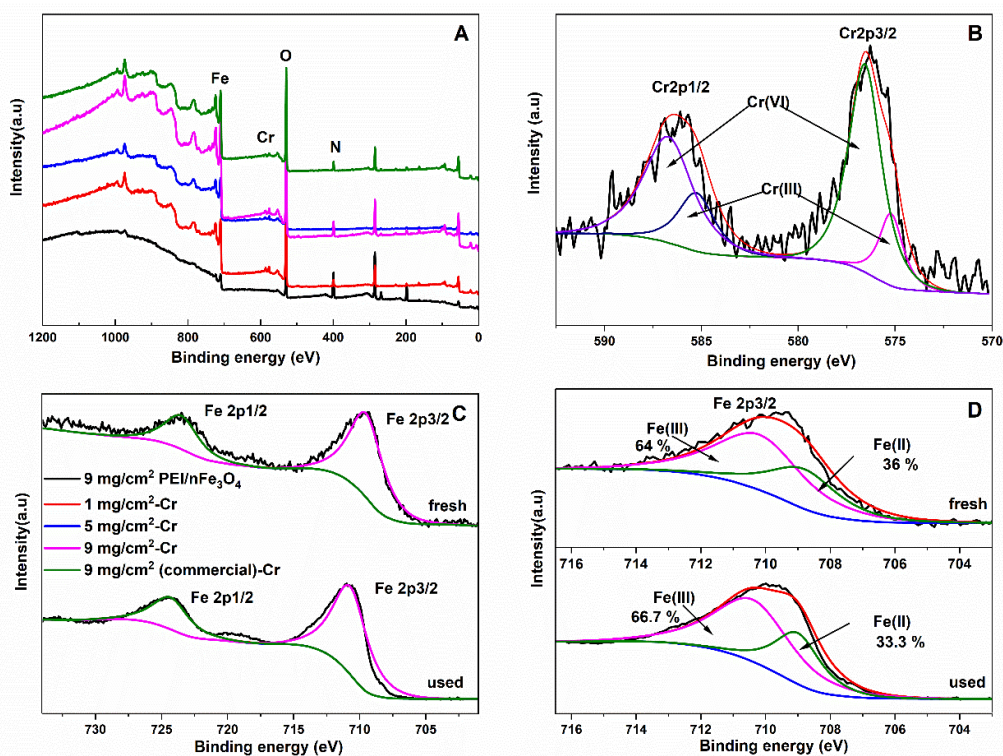


Figure 6. Results of the XPS analysis of the PEI/nFe₃O₄-9 ultrafiltration membrane.

The high-resolution XPS spectrum of the Cr 2p region exhibited four peaks. The peaks observed at 575.2 eV (Cr 2p_{3/2}) and 585.3 eV (Cr 2p_{1/2}) were assigned to Cr(III), whereas the peaks at 576.6 eV (Cr 2p_{3/2}) and 586.7 eV (Cr 2p_{1/2}) corresponded to Cr(VI)[53]. Similarly, chromium was detected in an EDS analysis (Fig. S1). This finding indicated the coexistence of Cr(III) and Cr(VI) on the surface of the modified membrane and confirmed the existence of the reaction pathway described by equations (4)-(7), suggesting that a reduction process was involved in the removal of Cr(VI).

The Fe 2p spectra also showed two peaks at 709.5 eV and 723.5 eV, which were assigned to Fe 2p_{3/2} and Fe 2p_{1/2}, respectively. These peaks corresponded to ferrous iron (Fe(II)) and ferric iron (Fe(III)) of the Fe₃O₄ nanoparticles, which was in agreement with the XRD results. Through analysis of the Fe 2p_{3/2} peaks and calculation of the relative areas for Fe(III) and Fe(II), the relative area ratio of Fe(III) to Fe(II) in the PEI/nFe₃O₄ ultrafiltration membrane after the experiment was found to be two times higher compared to a blank membrane. The shift of the peaks to higher binding energies was attributed to the conversion of Fe(II) to Fe(III) during the reduction process. Consequently, Fe(II) participated in the reduction of Cr(VI) by acting as an electron donor and resulted in the precipitation of Cr(III) on the

surface of the PEI/nFe₃O₄ membrane. Furthermore, the Fe 2p_{3/2} and Fe 2p_{1/2} peaks exhibited slight shifts, which could be attributed to the electrostatic interaction between Cr(VI) and nFe₃O₄ particles. The XPS analysis revealed the concurrent redox conversion of Cr(VI) and Fe(II) on the PEI/nFe₃O₄ ultrafiltration membrane, with the nitrogen-containing functional groups on PEI acting as the adsorption sites for Cr(VI).

The mechanism of Cr(VI) removal can be described as follows. Initially, negatively charged Cr(VI) ions (Cr₂O₇²⁻) are attracted to and adsorbed by the protonated amine groups on the surface of the modified membrane, and the nanoparticles within the pores. Subsequently, Cr(VI) is reduced to Cr(III) through the action of electron donors provided by Fe(II) and the amine groups [7]. The resulting Cr(III) species are then progressively removed from the solution through adsorption onto the PEI/nFe₃O₄ ultrafiltration membrane. This process of Cr(VI) removal involves redox reactions and electrostatic attraction, with additional forces such as hydrogen bonding and physical adsorption interactions also possibly playing a role [43].

3.6 Environmental implications of dynamic adsorption

The peristaltic pump-driven dynamic membrane adsorption achieved efficient and rapid removal efficiencies. Dynamic adsorption filtration driven by a peristaltic pump has advantages in terms of removal efficiency compared to static adsorption. The static adsorption efficiency of aminated-Fe₃O₄ nanoparticles-modified membrane has been reported to be only 0.325 mg/g-min [38]. Whereas, in this study, the PEI/nFe₃O₄-9 membrane achieved a comparable removal efficiency of 30.4 mg/g-min. Similarly, Jamshidifard et al. [54] used UiO-66-NH₂ MOF in polyacrylonitrile/chitosan nanofibers for static adsorption and membrane filtration treatment of Cr(VI), achieving a static adsorption efficiency of 1.228 mg/g-min and a dynamic adsorption efficiency of 4.975 mg/g-min. Fang et al. [55] developed a dynamic adsorption membrane with polydopamine nanoparticles for removing Pb(II), with a dynamic adsorption efficiency of 0.03 µg/g-min. Li and Yang [34] prepared electrospun chitosan nanofiber/polyester composite membranes for treating Cr(VI) wastewater, with a static adsorption efficiency of 0.074 mg/g-min and a dynamic adsorption efficiency of 0.099 mg/g-min.

The one-step dynamic adsorption and filtration mode driven by a peristaltic pump achieved a balance between removal efficiency and removal amount. Although the nitrogen-pressurized pure water flux was higher (PEI/nFe₃O₄-9: 572.2 LMH) compared to the peristaltic pump-driven dynamic adsorption and filtration mode (PEI/nFe₃O₄-9: 247.9 LMH), the latter demonstrated superior performance in terms of removal efficiency (Fig. 3).

The microporous structures and interlayer channels of the PEI/nFe₃O₄-9 ultrafiltration membrane, along with the lower membrane flux in dynamic adsorption and filtration mode, facilitated enhanced contact between Cr(VI) ions and nanoparticles, resulting in more effective removal of heavy metals. The slower peristaltic pump speed led to an extended retention time of pollutants in the membrane, thereby increasing the contact time between the Fe₃O₄ nanoparticles and the heavy metal ions. This prolonged interaction enhanced the adsorption efficiency of the surface-active sites, ultimately improving the removal efficiency of Cr(VI), which represents practical significance for various applications.

Notably, at pH 3, the PEI/nFe₃O₄-9 ultrafiltration membrane exhibited a remarkable removal efficiency of over 98%, meeting the effluent discharge standards set by many licensing authorities. Consequently, the developed PEI/nFe₃O₄ ultrafiltration membrane can serve as an efficient and easily separable membrane material for removing Cr(VI), particularly in environmental remediation targeting low-concentration chromium-containing wastewater. At the same time, the cost assessment of raw material consumption and the treatment of composites after adsorption are the remaining challenges of the study[56].

4. CONCLUSION

This study presents a novel approach for the removal of Cr(VI) using PEI/nFe₃O₄ ultrafiltration membranes, showcasing their high removal efficiency and practical applicability. Meanwhile, the peristaltic pump-driven one-step dynamic adsorption and filtration is a highly efficient mode. The lower peristaltic pump speed increases the contact time between contaminants and membrane materials, and increases the adsorption efficiency, resulting in higher Cr(VI) removal efficiency. The pH is a key factor affecting the adsorption effect, and PEI/nFe₃O₄-9 exhibited a high removal efficiency of 30.4 mg/g·min at pH 3, which was better than previous studies. At the same time, the effect of coexistence of other ions on the removal effect cannot be ignored. Phosphate ions have the greatest negative impact on the removal of Cr(VI), while Cl⁻ and NO₃⁻ had a slight influence due to their ability to enhance the reduction of Cr(VI) by nFe₃O₄.

SUPPLEMENTARY INFORMATION

Supplementary material is provided in a separate document.

Disclaimer (Artificial intelligence)

Option 1:

Author(s) hereby declare that NO generative AI technologies such as Large Language Models (ChatGPT, COPILOT, etc) and text-to-image generators have been used during writing or editing of manuscripts.

Option 2:

Author(s) hereby declare that generative AI technologies such as Large Language Models, etc have been used during writing or editing of manuscripts. This explanation will include the name, version, model, and source of the generative AI technology and as well as all input prompts provided to the generative AI technology

Details of the AI usage are given below:

- 1.
- 2.
- 3.

REFERENCE

1. Gu J, Chen H, Jiang F, et al. All-solid-state Z-scheme Co_9S_8 /graphitic carbon nitride photocatalysts for simultaneous reduction of Cr(VI) and oxidation of 2,4-dichlorophenoxyacetic acid under simulated solar irradiation. *Chemical Engineering Journal* 2019;360:1188-1198; doi: <https://doi.org/10.1016/j.cej.2018.10.137>.
2. Gong Y, Liu X, Huang L, et al. Stabilization of chromium: An alternative to make safe leathers. *Journal of Hazardous Materials* 2010;179(1):540-544; doi: <https://doi.org/10.1016/j.jhazmat.2010.03.037>.
3. Wang X, Wang T, Ma J, et al. Synthesis and characterization of a new hydrophilic boehmite-PVB/PVDF blended membrane supported nano zero-valent iron for removal of Cr(VI). *Separation and Purification Technology* 2018;205:74-83; doi: <https://doi.org/10.1016/j.seppur.2018.05.010>.
4. Costa M. Toxicity and carcinogenicity of Cr(VI) in animal models and humans. *Critical reviews in toxicology* 1997;27(5):431-442; doi: <https://doi.org/10.3109/10408449709078442>.
5. Adam MR, Salleh NM, Othman MHD, et al. The adsorptive removal of chromium (VI) in aqueous solution by novel natural zeolite based hollow fibre ceramic membrane. *Journal of Environmental Management* 2018;224:252-262; doi: <https://doi.org/10.1016/j.jenvman.2018.07.043>.
6. Peng H, Guo J. Removal of chromium from wastewater by membrane filtration, chemical precipitation, ion exchange, adsorption electrocoagulation, electrochemical reduction, electrodialysis, electrodeionization, photocatalysis and nanotechnology: a review. *ENVIRONMENTAL CHEMISTRY LETTERS* 2020;18(6):2055-2068; doi: <https://doi.org/10.1007/s10311-020-01058-x>.
7. Wang Z, Wang Y, Cao S, et al. Fabrication of core@shell structural $\text{Fe}-\text{Fe}_2\text{O}_3$ @PHCP nanochains with high saturation magnetization and abundant amino groups for hexavalent chromium adsorption and reduction. *Journal of Hazardous Materials* 2020;384:121483; doi: <https://doi.org/10.1016/j.jhazmat.2019.121483>.
8. Xu S, Xiao G, Wang Z, et al. A reusable chitosan/ TiO_2 @g- C_3N_4 nanocomposite membrane for photocatalytic removal of multiple toxic water pollutants under visible light. *WATER SCIENCE AND TECHNOLOGY* 2021;83(12):3063-3074; doi: <https://doi.org/10.2166/wst.2021.188>.
9. Yang X, Liu P, Yao M, et al. Mechanism and enhancement of Cr(VI) contaminated groundwater remediation by molasses. *Science of The Total Environment* 2021;780:146580; doi: <https://doi.org/10.1016/j.scitotenv.2021.146580>.
10. Zhao K, Ge L, Wong TI, et al. Gold-silver nanoparticles modified electrochemical sensor array for simultaneous determination of chromium(III) and chromium(VI) in wastewater samples. *Chemosphere* 2021;281:130880; doi: <https://doi.org/10.1016/j.chemosphere.2021.130880>.
11. Alyüz B, Veli S. Kinetics and equilibrium studies for the removal of nickel and zinc from aqueous solutions by ion exchange resins. *Journal of Hazardous Materials* 2009;167(1):482-488; doi:

- <https://doi.org/10.1016/j.jhazmat.2009.01.006>.
12. Ölmez T. The optimization of Cr(VI) reduction and removal by electrocoagulation using response surface methodology. *Journal of Hazardous Materials* 2009;162(2):1371-1378; doi: <https://doi.org/10.1016/j.jhazmat.2008.06.017>.
 13. Sharma D, Chaudhari PK, Prajapati AK. Removal of chromium (VI) and lead from electroplating effluent using electrocoagulation. *Separation Science and Technology* 2020;55(2):321-331; doi: <https://doi.org/10.1080/01496395.2018.1563157>.
 14. Saghi M, Shokri A, Arastehnodeh A, et al. The photo degradation of methyl red in aqueous solutions by α -Fe₂O₃/SiO₂ nano photocatalyst. *Journal of Nanoanalysis* 2018;5(3):163-170; doi: <https://doi.org/10.22034/JNA.2018.543608>.
 15. Karimi S, Shokri A. The removal of Hexavalent chromium;(Cr (VI)) by ZnO/LECA as a nano photocatalyst using full factorial experimental design, *J. Science of the Total Environment* 2021;8(3):167-175; doi: <http://doi.org/10.22034/jna.001>.
 16. Shokri A, Mahanpoor K. Removal of ortho-toluidine from industrial wastewater by UV/TiO₂ process. *Journal of Chemical Health Risks* 2016;6(3):213-223; doi: <https://sid.ir/paper/340299/en>.
 17. Shokri A. Degradation of 4-Nitrophenol from industrial wastewater by nano catalytic Ozonation. *International Journal of Nano Dimension (IJND)* 2016;7(2):160-167; doi: <https://sid.ir/paper/322309/en>.
 18. Shokri A, Joshagani AH. Using microwave along with TiO₂ for degradation of 4-chloro-2-nitrophenol in aqueous environment. *Russian Journal of Applied Chemistry* 2016;89(12):1985-1990; doi: <http://10.1134/S1070427216120090>.
 19. Shokri A, Mahanpoor K. Using UV/ZnO process for degradation of Acid red 283 in synthetic wastewater. *Bulgarian Chemical Communications* 2018;50(1):27-32.
 20. Feng X, Shang J, Chen J. Photoelectrocatalytic reduction of hexavalent chromium by Ti-doped hydroxyapatite thin film. *Molecular Catalysis* 2017;427:11-17; doi: <https://doi.org/10.1016/j.molcata.2016.09.031>.
 21. Feng Z-Q, Yuan X, Wang T. Porous polyacrylonitrile/graphene oxide nanofibers designed for high efficient adsorption of chromium ions (VI) in aqueous solution. *Chemical Engineering Journal* 2020;392:123730; doi: <https://doi.org/10.1016/j.cej.2019.123730>.
 22. Zhang L, Zeng Y, Cheng Z. Removal of heavy metal ions using chitosan and modified chitosan: A review. *Journal of Molecular Liquids* 2016;214:175-191; doi: <https://doi.org/10.1016/j.molliq.2015.12.013>.
 23. Hao M, Liu Y, Wu W, et al. Advanced porous adsorbents for radionuclides elimination. *EnergyChem* 2023;5(4):100101; doi: <https://doi.org/10.1016/j.enchem.2023.100101>.
 24. Khalili MS, Zare K, Moradi O, et al. Preparation and characterization of MWCNT–COOH–cellulose–MgO NP nanocomposite as adsorbent for removal of methylene blue from aqueous solutions: isotherm, thermodynamic and kinetic studies. *Journal of Nanostructure in Chemistry* 2018;8(1):103-121; doi: <http://doi.org/10.1007/s40097-018-0258-5>.
 25. Mohamed Khalith SB, Rishabb Anirud R, Ramalingam R, et al. Synthesis and characterization of magnetite carbon nanocomposite from agro waste as chromium adsorbent for effluent treatment. *Environmental Research* 2021;202:111669; doi: <https://doi.org/10.1016/j.envres.2021.111669>.
 26. Biswal SK, Panigrahi GK, Sahoo SK. Green synthesis of Fe₂O₃-Ag nanocomposite using Psidium guajava leaf extract: An eco-friendly and recyclable adsorbent for remediation of Cr(VI) from aqueous media. *Biophysical Chemistry* 2020;263:106392; doi: <https://doi.org/10.1016/j.bpc.2020.106392>.

27. Shrestha R, Ban S, Devkota S, et al. Technological trends in heavy metals removal from industrial wastewater: A review. *Journal of Environmental Chemical Engineering* 2021;9(4):105688; doi: <https://doi.org/10.1016/j.jece.2021.105688>.
28. Wang L, Li J, Jiang Q, et al. Water-soluble Fe₃O₄ nanoparticles with high solubility for removal of heavy-metal ions from waste water. *DALTON TRANSACTIONS* 2012;41(15):4544-4551; doi: <https://doi.org/10.1039/c2dt11827k>.
29. Beheshti H, Irani M, Hosseini L, et al. Removal of Cr (VI) from aqueous solutions using chitosan/MWCNT/Fe₃O₄ composite nanofibers-batch and column studies. *Chemical Engineering Journal* 2016;284:557-564; doi: <https://doi.org/10.1016/j.cej.2015.08.158>.
30. Wang H, Yuan X, Wu Y, et al. Facile synthesis of polypyrrole decorated reduced graphene oxide-Fe₃O₄ magnetic composites and its application for the Cr(VI) removal. *Chemical Engineering Journal* 2015;262:597-606; doi: <https://doi.org/10.1016/j.cej.2014.10.020>.
31. ZabihiSahebi A, Koushkbaghi S, Pishnamazi M, et al. Synthesis of cellulose acetate/chitosan/SWCNT/Fe₃O₄/TiO₂ composite nanofibers for the removal of Cr(VI), As(V), Methylene blue and Congo red from aqueous solutions. *International Journal of Biological Macromolecules* 2019;140:1296-1304; doi: <https://doi.org/10.1016/j.ijbiomac.2019.08.214>.
32. Tian Y, Ji C, Zhao M, et al. Preparation and characterization of baker's yeast modified by nano-Fe₃O₄: Application of biosorption of methyl violet in aqueous solution. *Chemical Engineering Journal* 2010;165(2):474-481; doi: <https://doi.org/10.1016/j.cej.2010.09.037>.
33. Li L, Zhu Z, Shi J, et al. Simultaneous phosphorus removal and adsorbents recovery with Ca-PAC assisted adsorption dynamic membrane system: Removal performance and influencing factors. *Journal of Cleaner Production* 2023;384:135591; doi: <https://doi.org/10.1016/j.jclepro.2022.135591>.
34. Li L, Li Y, Yang C. Chemical filtration of Cr (VI) with electrospun chitosan nanofiber membranes. *Carbohydrate Polymers* 2016;140:299-307; doi: <https://doi.org/10.1016/j.carbpol.2015.12.067>.
35. Vo TS, Hossain MM, Jeong HM, et al. Heavy metal removal applications using adsorptive membranes. *NANO CONVERGENCE* 2020;7(1); doi: <https://doi.org/10.1186/s40580-020-00245-4>.
36. Zhu F, Zheng Y-M, Zhang B-G, et al. A critical review on the electrospun nanofibrous membranes for the adsorption of heavy metals in water treatment. *Journal of Hazardous Materials* 2021;401:123608; doi: <https://doi.org/10.1016/j.jhazmat.2020.123608>.
37. Koushkbaghi S, Jafari P, Rabiei J, et al. Fabrication of PET/PAN/GO/Fe₃O₄ nanofibrous membrane for the removal of Pb(II) and Cr(VI) ions. *Chemical Engineering Journal* 2016;301:42-50; doi: <https://doi.org/10.1016/j.cej.2016.04.076>.
38. Koushkbaghi S, Zakialamdari A, Pishnamazi M, et al. Aminated-Fe₃O₄ nanoparticles filled chitosan/PVA/PES dual layers nanofibrous membrane for the removal of Cr(VI) and Pb(II) ions from aqueous solutions in adsorption and membrane processes. *Chemical Engineering Journal* 2018;337:169-182; doi: <https://doi.org/10.1016/j.cej.2017.12.075>.
39. Park JE, Shin J-H, Oh W, et al. Removal of Hexavalent Chromium(VI) from Wastewater Using Chitosan-Coated Iron Oxide Nanocomposite Membranes. *TOXICS* 2022;10(2); doi: <https://doi.org/10.3390/toxics10020098>.
40. Yilimulati M, Wang L, Ma X, et al. Adsorption of ciprofloxacin to functionalized nano-sized polystyrene plastic: Kinetics, thermochemistry and toxicity. *Science of The Total Environment* 2021;750:142370; doi: <https://doi.org/10.1016/j.scitotenv.2020.142370>.

41. Yang X, Liu Y, Hu S, et al. Construction of Fe₃O₄@MXene composite nanofiltration membrane for heavy metal ions removal from wastewater. *POLYMERS FOR ADVANCED TECHNOLOGIES* 2021;32(3):1000-1010; doi: <https://doi.org/10.1002/pat.5148>.
42. Raganati F, Alfe M, Gargiulo V, et al. Kinetic study and breakthrough analysis of the hybrid physical/chemical CO₂ adsorption/desorption behavior of a magnetite-based sorbent. *Chemical Engineering Journal* 2019;372:526-535; doi: <https://doi.org/10.1016/j.cej.2019.04.165>.
43. Luo L, Cai W, Zhou J, et al. Facile synthesis of boehmite/PVA composite membrane with enhanced adsorption performance towards Cr(VI). *Journal of Hazardous Materials* 2016;318:452-459; doi: <https://doi.org/10.1016/j.jhazmat.2016.07.019>.
44. Dong L, Liang J, Li Y, et al. Effect of coexisting ions on Cr(VI) adsorption onto surfactant modified *Auricularia auricula* spent substrate in aqueous solution. *Ecotoxicology and Environmental Safety* 2018;166:390-400; doi: <https://doi.org/10.1016/j.ecoenv.2018.09.097>.
45. Yao Z, Du S, Zhang Y, et al. Positively charged membrane for removing low concentration Cr(VI) in ultrafiltration process. *Journal of Water Process Engineering* 2015;8:99-107; doi: <https://doi.org/10.1016/j.jwpe.2015.08.005>.
46. Reddad Z, Gerente C, Andres Y, et al. Mechanisms of Cr(III) and Cr(VI) removal from aqueous solutions by sugar beet pulp. *ENVIRONMENTAL TECHNOLOGY* 2003;24(2):257-264; doi: <https://doi.org/10.1080/09593330309385557>.
47. Sciscenko I, Luca V, Ramos CP, et al. Immobilization of nanoscale zerovalent iron in hierarchically channelled polyacrylonitrile for Cr(VI) remediation in wastewater. *Journal of Water Process Engineering* 2021;39:101704; doi: <https://doi.org/10.1016/j.jwpe.2020.101704>.
48. Su J, Hao H, Lv X, et al. Properties and mechanism of hexavalent chromium removal by FeS@ graphite carbon nitride nanocomposites. *Colloids and Surfaces A: Physicochemical and Engineering Aspects* 2020;597:124751; doi: <https://doi.org/10.1016/j.colsurfa.2020.124751>.
49. Zhao R, Li Y, Li X, et al. Facile hydrothermal synthesis of branched polyethylenimine grafted electrospun polyacrylonitrile fiber membrane as a highly efficient and reusable bilirubin adsorbent in hemoperfusion. *Journal of Colloid and Interface Science* 2018;514:675-685; doi: <https://doi.org/10.1016/j.jcis.2017.12.059>.
50. Liu J, Wen Y, Mo Y, et al. Chemical speciation determines combined cytotoxicity: Examples of biochar and arsenic/chromium. *Journal of Hazardous Materials* 2023;448:130855; doi: <https://doi.org/10.1016/j.jhazmat.2023.130855>.
51. Park SJ, Jang YS. Pore structure and surface properties of chemically modified activated carbons for adsorption mechanism and rate of Cr(VI). *JOURNAL OF COLLOID AND INTERFACE SCIENCE* 2002;249(2):458-463; doi: <https://doi.org/10.1006/jcis.2002.8269>.
52. Tobin JM, Cooper DG, Neufeld RJ. Uptake of Metal Ions by *Rhizopus arrhizus* Biomass. *Applied and environmental microbiology* 1984;47(4):821-824; doi: <https://doi.org/10.1128/AEM.47.4.821-824.1984>.
53. Zhao R, Li X, Li Y, et al. Functionalized magnetic iron oxide/polyacrylonitrile composite electrospun fibers as effective chromium (VI) adsorbents for water purification. *Journal of Colloid and Interface Science* 2017;505:1018-1030; doi: <https://doi.org/10.1016/j.jcis.2017.06.094>.
54. Jamshidifard S, Koushkbaghi S, Hosseini S, et al. Incorporation of UiO-66-NH₂ MOF into the PAN/chitosan nanofibers for adsorption and membrane filtration of Pb(II), Cd(II) and Cr(VI) ions from aqueous solutions. *Journal of Hazardous Materials* 2019;368:10-20; doi:

<https://doi.org/10.1016/j.jhazmat.2019.01.024>.

55. Fang X, Li J, Li X, et al. Internal pore decoration with polydopamine nanoparticle on polymeric ultrafiltration membrane for enhanced heavy metal removal. Chemical Engineering Journal 2017;314:38-49; doi: <https://doi.org/10.1016/j.cej.2016.12.125>.
56. Shokri A, Sanavi Fard M. Techno-economic assessment of water desalination: Future outlooks and challenges. Process Safety and Environmental Protection 2023;169:564-578; doi: <https://doi.org/10.1016/j.psep.2022.11.007>.

UNDER PEER REVIEW